Western University
Scholarship@Western

Chemistry Publications Chemistry Department

2021

Band-Gap Tuning in Acceptor-Donor-Acceptor Boron Difluoride Formazanates

Francis L. Buguis

Michael Anghel

Joe B. Gilroy
Univeristy of Western Ontario, joe.gilroy@uwo.ca

Jasveer S. Dhindsa

Follow this and additional works at: https://ir.lib.uwo.ca/chempub

Part of the Chemistry Commons

Citation of this paper:
Buguis, Francis L.; Anghel, Michael; Gilroy, Joe B.; and Dhindsa, Jasveer S., "Band-Gap Tuning in Acceptor-Donor-Acceptor Boron Difluoride Formazanates" (2021). *Chemistry Publications*. 236.
https://ir.lib.uwo.ca/chempub/236

Band-Gap Engineering in Acceptor-Donor-Acceptor Boron Difluoride Formazanates

Jasveer S. Dhindsa, Francis L. Buguis, Michael Anghel, and Joe B. Gilroy*

Department of Chemistry and the Centre for Advanced Materials and Biomaterials Research (CAMBR), The University of Western Ontario, London, ON, Canada, N6A 5B7.

ORCID

Jasveer S. Dhindsa: https://orcid.org/0000-0003-0754-7757

Francis L. Buguis: https://orcid.org/0000-0002-7247-3769

Joe B. Gilroy: https://orcid.org/0000-0003-0349-7780

TOC ENTRY

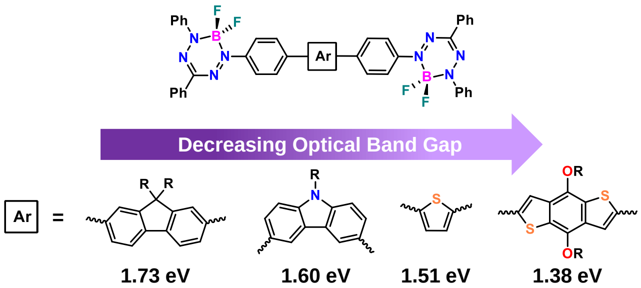

ABSTRACT

π-Conjugated molecules with acceptor-donor-acceptor (A-D-A) electronic structures are an important class of materials due to their tunable optoelectronic properties and applications in, for example, organic light-emitting diodes, nonlinear optical devices, and organic solar cells. The frontier molecular orbital energies, and thus band gaps, of these materials can be tuned by varying the donor and acceptor traits and π-electron counts of the structural components. Herein, we report the synthesis and characterization of a series of A-D-A compounds consisting of BF_2 formazanates as electron acceptors bridged by a variety of π-conjugated donors. The results, which are supported by DFT calculations, demonstrate rational control of optoelectronic properties and the ability to tune the corresponding band gaps. The narrowest band gaps (E_g^{Opt} = 1.38 eV and E_g^{CV} = 1.21 eV) were observed when BF_2 formazanates and benzodithiophene units were combined. This study provides significant insight into the band-gap engineering of materials derived from BF_2 formazanates and will inform their future development as semiconductors for use in organic electronics.

INTRODUCTION

π-Conjugated molecules whose optical and electrochemical properties can be tuned through molecular engineering are an intriguing class of materials due to their applications in semiconducting devices such as field-effect transistors,[1] light-emitting diodes,[2] and organic solar cells (OSCs).[3] One strategy to tune the frontier molecular orbital energies and band gaps[4] of π-conjugated molecules is the creation of donor-acceptor (D-A) interactions.[5] The highest occupied molecular orbital (HOMO) and the lowest unoccupied molecular orbital (LUMO) energies of such systems can be altered by incorporating D and A units, with varying electron donating and withdrawing abilities, into π-conjugated scaffolds.[5-6] Generally, the HOMO is dependent on the electron density and delocalization of electrons throughout the π-conjugated system.[6] Therefore, synthesizing molecules with large π-electron systems and introducing heteroatoms such as N, O, and S are strategies that lead to altered electronic structures that often increase HOMO energies.[5, 7] Conversely, incorporating electron-withdrawing units such as −F, −Cl, and −C≡N often lowers both HOMO and LUMO energies.[5, 7]

D-A compounds can be classified into several types: D-A, D-π-A, D-A-D, D-π-A-π-D, A-D-A, A-π-D-π-A, etc.[8] Recently, A-D-A compounds have attracted significant attention as a result of their lower frontier orbital energies and tendency to increase exciton separation and charge transport compared to D-A-D architectures.[9] These compounds have found applications, for example, in nonlinear optical devices,[10] as emissive layers in organic light-emitting diodes (*e.g.*, **1**),[11] as efficient thermally-activated delayed fluorophores (*e.g.*, **2**),[12] as ratiometric temperature and viscosity sensors,[13] as photothermal therapeutics,[14] and most commonly in OSCs.[9] Initially, A-D-A compounds were used as donors in combination with fullerene acceptors in OSCs.[15] In the last 5−6 years, however, A-D-A systems have been used as alternatives to fullerene acceptors,[9, 16] and power conversion efficiencies have now reached 18% for OSCs based on A-D-A acceptor **3**.[16d]

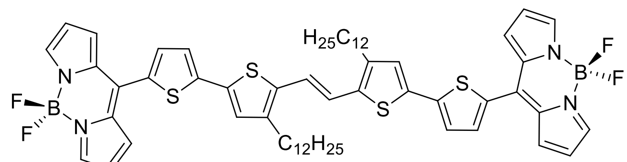

1

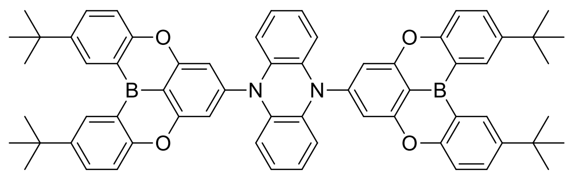

2

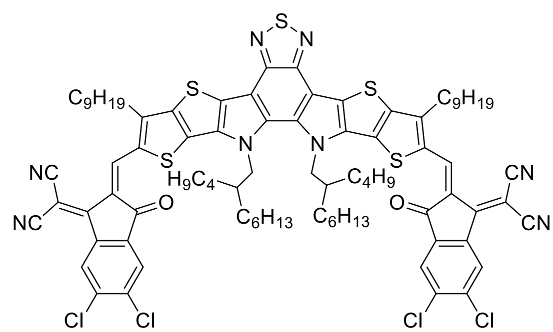

3

The purpose of this work is to explore the properties of a novel series of π-conjugated A-D-A type compounds using BF_2 complexes (*e.g.*, **BF_2**), derived from formazans (*e.g.*, **Fz**), as acceptors. Molecular and polymer materials derived from BF_2 formazanates are readily accessible and exhibit tunable absorption, emission, and redox properties, making them strong candidates for use in a variety of organic electronics.[17] These properties can be tuned by varying the substituents at the *para*-position of the *N*-aryl rings[18] and by the extension of π-conjugation.[19] BF_2 formazanates have found application as fluorescence cell-imaging agents,[18c] cancer theranostics,[20] near-infrared emitters,[21] electrochemiluminescent materials,[22] multifunctional polymers,[19, 23] and as precursors to unusual BN heterocycles.[24] Recently, a BF_2 formazanate capped with *N*-annulated perylene diimides **4** was used as an electron acceptor in OSCs.[25] The incorporation of the BF_2 formazanate core enabled tuning of the LUMO energy and led to near-panchromatic absorption.[25] BF_2 formazanates have also been incorporated into various D-A-D π-conjugated structures. For example, copper-assisted azide-alkyne cycloaddition reactions were used to produce compound **5** along with model compounds using alkylated fluorenes as electron donors and BF_2 formazanates as electron acceptors.[23] Thorough examination of the model compounds revealed that the π-conjugation involving BF_2 formazanate units did not extend beyond the triazole rings formed in these systems.[23] More recently, a team led by Tanaka and Chujo synthesized fluorene end-capped D-A-D compound **6** and similar polymers using Stille cross-coupling reactions.[19c] A red shift of 108 nm in the wavelength of maximum absorption (λ_{max}) of **6** was observed when compared to the parent BF_2 formazanate.[19c] The Zade group synthesized thiophene and 3,4-ethylenedioxythiophene D-A-D BF_2 formazanates with optical band gaps (E_g^{Opt}) of 1.80 and 1.70 eV, respectively.[19b] Despite the advances in D-A-D BF_2 formazanate chemistry, analogous A-D-A structures have not yet been explored.

Herein, we demonstrate that band gaps (*i.e.*, HOMO−LUMO gaps) of A-D-A BF_2 formazanates can be readily and rationally tuned by variation of the bridging donor unit. Specifically, we paired BF_2 formazanate acceptors and common donors such as thiophene (TH), alkylated fluorene (FL) and carbazole (CBZ), and alkoxylated benzodithiophene (BDT) and explored their optical and electrochemical properties both experimentally and computationally.

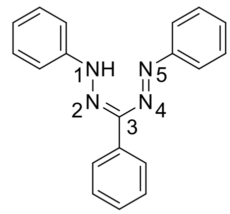

Fz

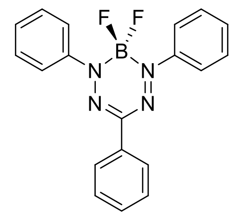

BF_2

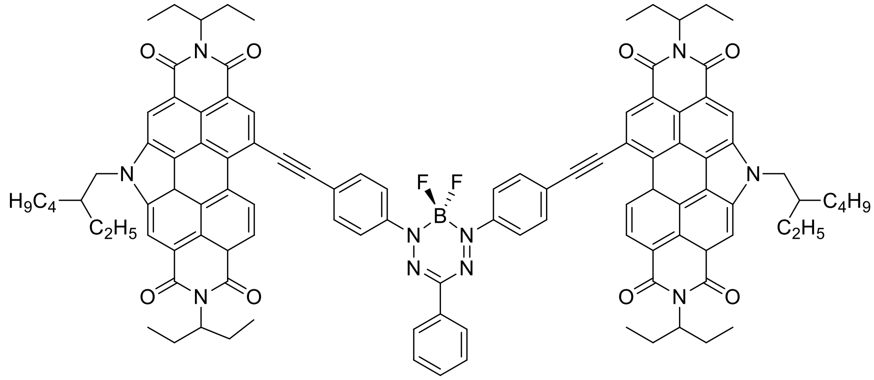

4

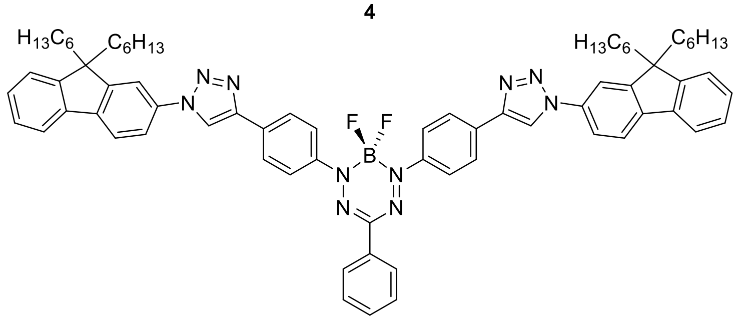

5

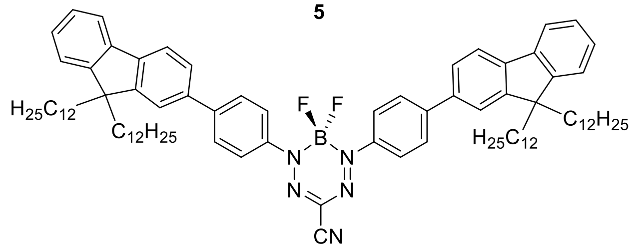

6

RESULTS AND DISCUSSION

Synthesis

A series of A-D-A BF_2 formazanates were synthesized using palladium-catalyzed Stille cross-coupling reactions. Our approach began with the synthesis of 1-(*p*-bromobenzene)-3,5-diphenyl formazan (**Fz-Br**) under biphasic conditions by adapting a known procedure.[26] Briefly, a coupling reaction between the *p*-bromobenzenediazonium chloride and 1,3-diphenyl hydrazone afforded

Fz-Br in 73% yield.[26] The structure of **Fz-Br** was confirmed by the observation of a characteristic NH signal at 15.35 ppm in its ^{1}H NMR spectrum (Figures S1 and S2). A solution of **Fz-Br** in toluene was then heated to reflux in the presence of excess BF_3•OEt_2 and NEt_3 for 16 h which gave the BF_2 formazanate **BF_2-Br** in 55% yield after purification by column chromatography (Figures S3−S5). The formation of dimeric compound **BF_2-BF_2** and A-D-A compounds were catalyzed by $Pd_2(dba)_3$ in the presence of P(*o*-tol)$_3$. The reaction of **BF_2-Br** with hexamethylditin for 15 min at 170 °C in a sealed pressure tube (pressure = 3.5 bar) resulted in the formation of the dimeric compound (**BF_2-BF_2**) in 29% yield (Scheme 1a, Figures S6−S8). The monomeric model compound **BF_2** and the diyne-bridged compound **BF_2-DY-BF_2** (Scheme 1b) were prepared according to published procedures.[19a, 27]

To prepare A-D-A compounds, we targeted common donors such as TH[28] and FL[29] as the properties of donor units can be tuned by incorporating heteroatoms such as N, O and S into the molecular skeleton.[7] CBZ units are stronger electron-donors than FL due to the delocalization of the lone pair on nitrogen participating in the π-electron system, giving subsequent compounds unique optical and electrochemical properties compared to FL.[30] BDT possesses a planar conjugated structure and has been commonly used as a donor unit in D-A polymers and small molecules for use in OSCs.[31] Due to their structural symmetry and fused aromatic structure, BDT-containing compounds tend to π-stack in the solid state often enhancing charge-transport properties.[31c] The reaction of **BF_2-Br** with distannyl derivatives of TH, FL, CBZ, and BDT for 15 min at 170 °C (pressure = 3.2–4.9 bar) resulted in the formation of A-D-A compounds in purified yields ranging from 48 to 74% (Scheme 1c, Figures S9−S22). It is noteworthy that compared to previous reports of Stille cross-coupling reactions for BF_2 formazanates, we have drastically reduced reaction times from 16–48 h for conventional reflux reactions[19b, 19c] to 15 min by superheating in sealed glass tubes.

All compounds reported here can be handled and manipulated under ambient conditions and are stable in solution and the solid state for several weeks. Their molecular structures were confirmed by multinuclear NMR and IR spectroscopy and mass spectrometry. Our efforts to grow single crystals suitable for X-ray diffraction studies of the compounds reported were unsuccessful, with most compounds tending to form films.

Scheme 1. Synthesis of (a) BF_2-BF_2, (b) BF_2-DY-BF_2, and (c) A-D-A BF_2 Formazanates.

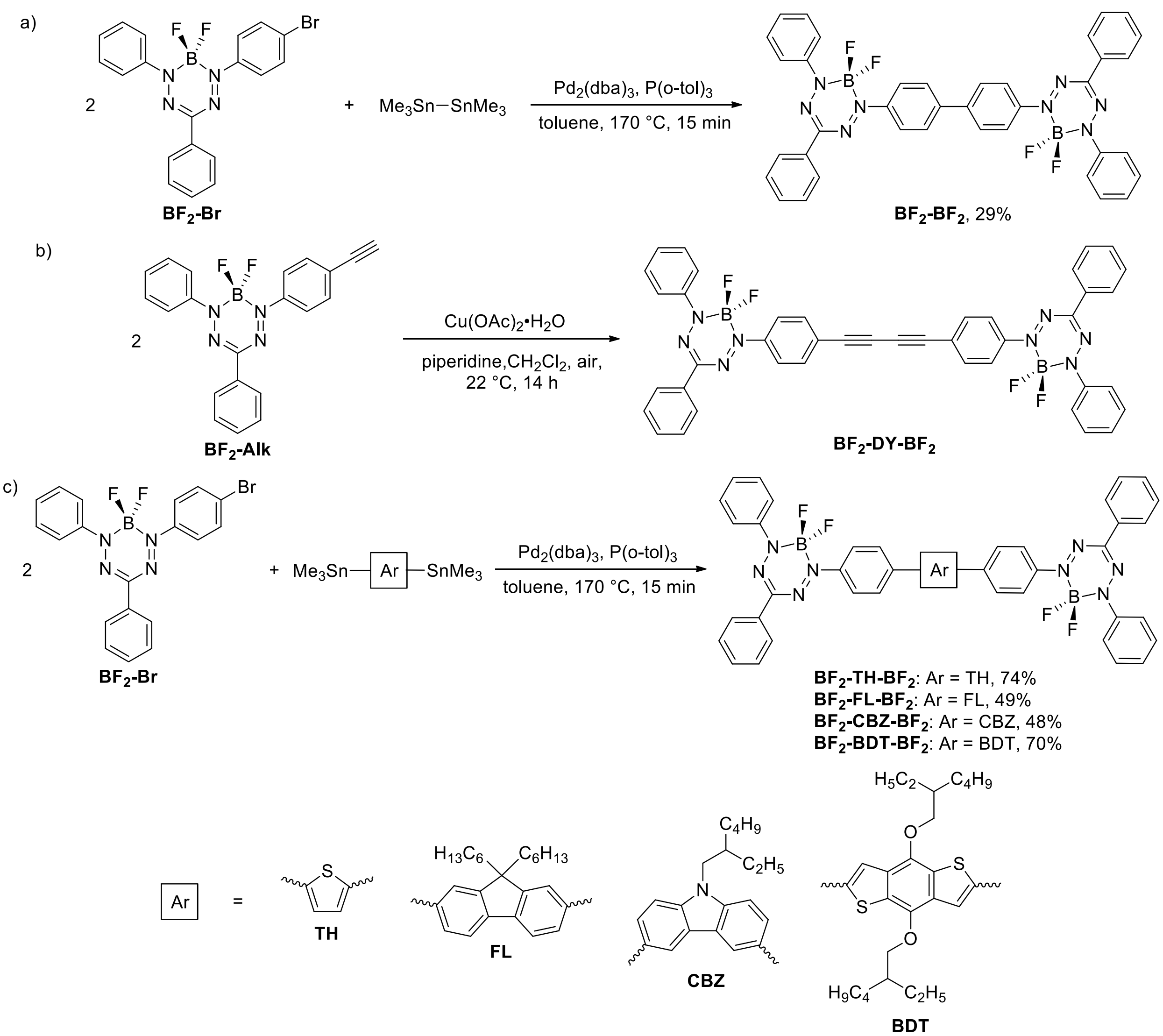

Density Functional Theory

To gain insight into the electronic structures of A-D-A BF_2 formazanates and related model systems, we used density-functional theory (DFT) to calculate the frontier molecular orbitals at the optimized ground-state geometries with alkyl chains approximated as methyl groups. The DFT calculations were performed using a LC-ωhPBE/DGDZVP2[32] method with a tuned range-separation parameter ω = 0.14. These parameters were optimized previously for similar compounds with large π-electron systems and significant charge-transfer character.[21] Time-dependent DFT (TDDFT) calculations implicate the HOMO (π type) and LUMO (π* type) as the orbital pair that makes the dominant contribution to the low-energy absorption bands for these compounds (see below for details). Both the HOMOs and LUMOs of **BF_2-BF_2**, **BF_2-DY-BF_2**, and **BF_2-TH-BF_2** are delocalized throughout the entire compound (Figure 1). The HOMOs of **BF_2-FL-BF_2**, **BF_2-CBZ-BF_2**, and **BF_2-BDT-BF_2** are centred on the electron-donating bridging units with minimal contribution from the BF_2 formazanate units. The LUMOs are localized on the BF_2 formazanate units suggesting that the lowest-energy excitation for these compounds has significant charge-transfer character (Figure 1). From these calculations we were able to group these compounds into two series: i) compounds with low-energy electronic excitations involving limited or no charge-transfer character (**BF_2-BF_2**, **BF_2-DY-BF_2**, and **BF_2-TH-BF_2**), and ii) compounds whose low-energy electronic excitations have significant charge-transfer character (**BF_2-FL-BF_2**, **BF_2-CBZ-BF_2**, and **BF_2-BDT-BF_2**).

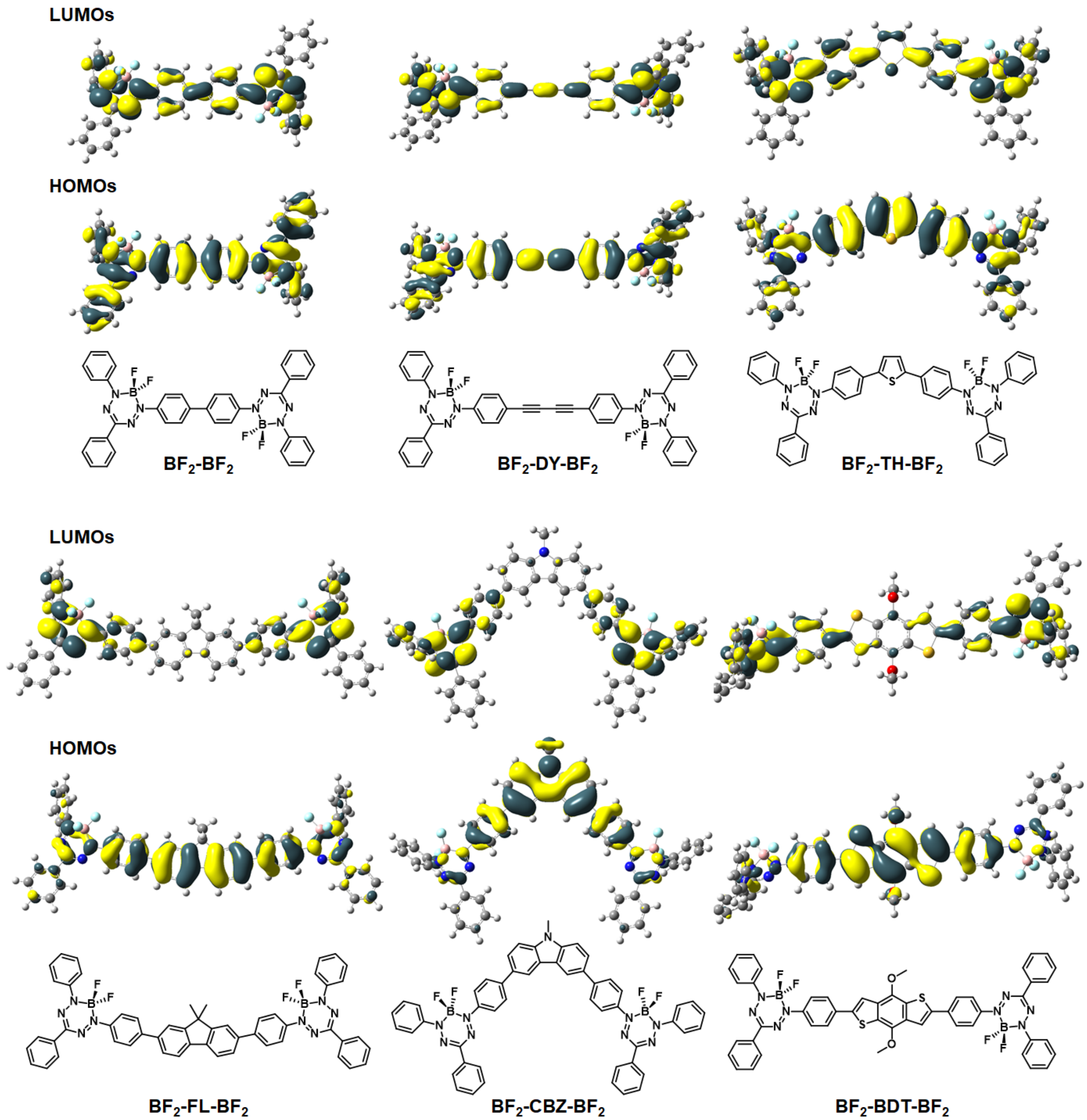

Figure 1. Frontier molecular orbitals of A-D-A BF_2 formazanates calculated at the ground-state geometries using the LC-ωhPBE(ω=0.14)/DGDZVP2 SCRF = (PCM, Solvent = CH_2Cl_2) method. Alkyl chains are approximated as methyl groups.

UV-Visible Absorption Spectroscopy

The optical properties of A-D-A BF_2 formazanates and related model systems were explored by recording the UV-vis absorption spectra in CH_2Cl_2 and as thin films (Figure 2, and Table 1). Each compound in the series is strongly absorbing with low-energy wavelength of maximum absorption (λ_{max}) between 509 and 596 nm in CH_2Cl_2 and between 528 and 645 nm as thin films. Comparing the first series of compounds (**BF$_2$-BF$_2$**, **BF$_2$-DY-BF$_2$**, and **BF$_2$-TH-BF$_2$**) to the model compound **BF$_2$**, a significant change in properties was observed upon extension of the π-electron system through the different spacers. The dimeric compound **BF$_2$-BF$_2$** (λ_{max} = 570 nm in CH_2Cl_2) and **BF$_2$-DY-BF$_2$** (λ_{max} = 564 nm) had lower energy λ_{max} compared to **BF$_2$** (λ_{max} = 509 nm). The λ_{max} of **BF$_2$-TH-BF$_2$** was further red-shifted, by 87 nm compared to **BF$_2$**, likely due to the electron-donating character of the thiophene spacer.[28, 33] The molar absorptivity of **BF$_2$-BF$_2$** (ε = 47,300 M^{-1} cm^{-1}) and the A-D-A compounds (ε = 46,400−58,200 M^{-1} cm^{-1}) are approximately doubled compared to **BF$_2$** (ε = 23,400 M^{-1} cm^{-1}) due to the presence of two BF_2 formazanate units in each molecule. The second series of compounds (**BF$_2$-FL-BF$_2$**, **BF$_2$-CBZ-BF$_2$, BF$_2$-BDT-BF$_2$**) also exhibited lower energy λ_{max} values ($\Delta\lambda_{max}$ = 51–83 nm) compared to the model compound **BF$_2$** with **BF$_2$-BDT-BF$_2$** having the lowest-energy absorption band. Compared to the analogous D-A-D compound (λ_{max} = 570 nm, ε = 20,511 M^{-1} cm^{-1} in CH_3CN),[19b] the absorption band observed for the A-D-A compound **BF$_2$-TH-BF$_2$** appeared at lower energy (λ_{max} = 596 nm, ε = 52,400 M^{-1} cm^{-1} in CH_2Cl_2). In contrast, the absorption band observed for **BF$_2$-FL-BF$_2$** (λ_{max} = 560 nm, ε = 58,200 M^{-1} cm^{-1} in CH_2Cl_2) appeared at higher energy than compound **6** (λ_{max} = 612 nm, ε = 36,000 M^{-1} cm^{-1} in toluene), which is based on a 3-cyanoformazanate ligand.[19c] In both cases, the molar absorptivities of the A-D-A systems were dramatically higher than those of the analogous D-A-D systems due to the presence of two BF_2 formazanate units per molecule.

BF_2 complexes of triarylformazanates tend to be weakly emissive as a result of free rotation of the aryl substituents at nitrogen and carbon activating non-radiative decay pathways.[18b] This trend is consistent with our observations for the compounds described here, where emission responses were detectable in some cases, but very weak (Figure S23). This was in contrast to recently reported BF_2 complexes of 3-cyanoformazanates that exhibited strong near-infrared emission.[19c]

In all cases, TDDFT calculations were used to estimate the lowest-energy excitation energies in CH_2Cl_2 (primarily HOMO−LUMO character) using the LC-ωhPBE(ω=0.14)/DGDZVP2 method (Table 1). The calculated low-energy excitation wavelengths agreed within 12−36 nm of their respective experimental values, and were consistent with qualitative trends (Table 1). The charge-transfer character implied by the calculated frontier orbitals was corroborated by the fact that functionals such as PBE0[34] underestimated the relevant low-energy excitation energies (Table S1).

To gain insight into the relationship between molecular structure and photophysical properties, we investigated the structural metrics of the ground-state geometries obtained by DFT calculations (Figure S24). We compared the angles between the planes defined by the *N*-bound benzene ring of both BF_2 formazanates in the case of **BF_2-BF_2** and **BF_2-DY-BF_2** or the angle between the planes defined by the *N*-bound benzene ring of the BF_2 formazanate and the neighbouring aryl rings of the spacers (TH, FL, CBZ, BDT). The angles extracted for **BF_2-DY-BF_2**, **BF_2-TH-BF_2**, and **BF_2-BDT-BF_2** were between 0.9° and 3.3° and for **BF_2-BF_2**, **BF_2-FL-BF_2**, and **BF_2-CBZ-BF_2** were between 28.3° and 31.2° suggesting that the former set of compounds have enhanced planarity. This is due to the fact that a five-membered thiophene ring (or alkyne) attached to a benzene ring introduces less steric encumbrance compared to two sixmembered benzene rings attached to one another.[35] As a result, despite having a smaller π-electron system, the planar **BF_2-TH-BF_2** has a red-shifted low-energy absorption band compared to **BF_2-FL-BF_2** and **BF_2-CBZ-BF_2**.

Thin films were prepared by spin-coating $CHCl_3$ solutions of the respective compounds on quartz slides. The absorption spectra of these films featured broadened and red-shifted absorption bands compared to the solution spectra (Figure 2, Table 1). The thin-film spectrum of **BF_2-BDT-BF_2** revealed two additional shoulders at higher wavelengths (685 nm and 772 nm) due to strong intermolecular π-π interactions in the solid state.[15d, 36] The optical band gaps (E_g^{opt}) were estimated from the onset of absorption, according to the equation $E_g^{Opt} = 1240/\lambda_{abs}^{onset}$ (Table 1). Most notably, a decrease in E_g^{opt} was observed from 1.89 eV for monomeric compound **BF_2** to 1.73 eV for **BF_2-FL-BF_2**, 1.60 eV for **BF_2-CBZ-BF_2**, and 1.39 eV for **BF_2-BDT-BF_2**.

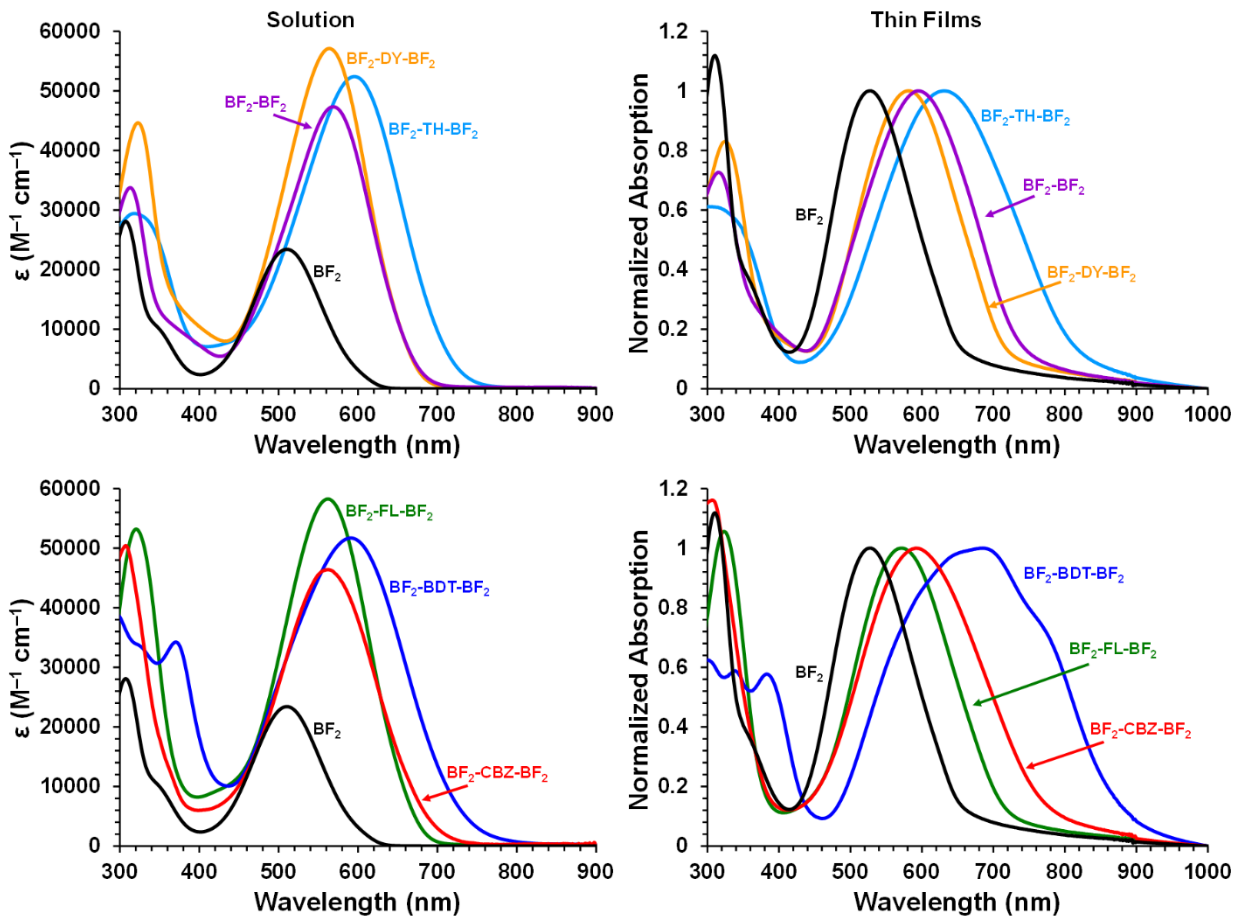

Figure 2. UV-vis absorption spectra in CH_2Cl_2 solutions and as thin films.

Table 1. Experimental and Calculated UV-Vis Absorption Spectral Data.

	CH_2Cl_2			Thin Film		
	Experiment		Theory	Experiment		
	λ_{max} (nm)	ε (M^{-1} cm^{-1})	λ_{max} (nm)^a	λ_{max} (nm)	λ_{abs}^{onset} (nm)	E_g^{Opt} (eV)^b
BF_2	509	23,400	492	528	656	1.89
BF_2-BF_2	570	47,300	534	595	742	1.67
BF_2-DY-BF_2	564	57,100	552	581	720	1.72
BF_2-TH-BF_2	596	52,400	569	632	820	1.51
BF_2-FL-BF_2	560	58,200	527	572	715	1.73
BF_2-CBZ-BF_2	563	46,400	538	593	776	1.60
BF_2-BDT-BF_2	592	51,700	557	645	895	1.38

^{a}Theoretical values were obtained using TDDFT at the LC-ωhPBE (ω=0.14)/DGDZVP2 level with non-equilibrium solvation (CH_2Cl_2). $^b E_g^{opt} = 1240/\lambda_{abs}^{onset}$.

Cyclic Voltammetry

Cyclic voltammograms collected in CH_2Cl_2 solutions are shown in Figure 3 and the data are summarized in Table 2. The cyclic voltammetry (CV) data collected from these series of compounds reveal several trends. Each of the compounds exhibit two reduction waves which correspond to the reversible formation of radical anions (E_{red1} = −0.83 to −0.94 V relative to the Fc/Fc$^+$ redox couple) and the irreversible formation of dianions (E_{red2} = −1.82 to −1.99 V). The current response associated with these waves corresponds to one electron per BF_2 formazanate unit. The first reduction event observed for **BF_2-BF_2** is split into two overlapping waves suggesting the successive reduction of each BF_2 formazanate unit and implying enhanced electronic communication between BF_2 formazanate units compared to the A-D-A systems. In addition to these reduction waves, A-D-A compounds **BF_2-TH-BF_2**, **BF_2-FL-BF_2**, **BF_2-CBZ-BF_2**, and **BF_2-BDT-BF_2** also exhibited two reversible one-electron oxidation waves corresponding to the formation of their radical cation (E_{ox1} = 0.46 to 1.01 V) and dication (E_{ox2} = 0.86 to 1.13 V) forms. Similar oxidation events were not observed for **BF_2**, **BF_2-BF_2**, and **BF_2-DY-BF_2**. Rather, irreversible oxidation waves were observed for these compounds near the edge of the solvent window (E_{onset}^{ox} = 1.04 to 1.12 V). HOMO and LUMO energies were estimated from the onset of E_{ox1} and E_{red1} respectively, according to the equations ($E_{LUMO} = −5.1 – E_{onset}^{red}$ and $E_{HOMO} = −5.1 – E_{onset}^{ox}$) and the data are summarized in Figure 4. In most cases, the LUMO energies were similar (−4.24 to −4.26 eV) with the exception of **BF_2-BF_2** (−4.33 eV) and **BF_2-DY-BF_2** (−4.35 eV) which have a higher degree of delocalization in their LUMOs that results in slightly lower energies. This confirms that the LUMOs are primarily centred on the BF_2 formazanate units. The HOMO energies, however, are strongly dependent on the identity of the bridging donor unit. For example, **BF_2-CBZ-BF_2** has a higher HOMO energy (−5.77 eV), and thus a narrower electrochemical band gap (E_g^{CV} = 1.53 eV), compared to **BF2-FL-BF2** (E_{HOMO} = −5.96 eV, E_g^{CV} = 1.71 eV) due to the stronger electron-donating character of CBZ compared to FL. **BF2-BDT-BF2** has the highest HOMO energy (−5.47 eV) and the smallest E_g^{CV} (1.21 eV) owing to a large π-electron system and strong donor-acceptor interaction whereas, the monomeric compound **BF2** has the lowest HOMO energy (−6.22 eV) and the largest E_g^{CV} (1.98 eV).

In all cases, there is a good agreement between E_g^{Opt} and E_g^{CV} and the differences are within 0.02−0.17 eV. A direct comparison of the first series of compounds reveals a decrease in band gap is observed from **BF2**, to **BF2-DY-BF2**, **BF2-BF2**, and **BF2-TH-BF2**. The second series of compounds involves a decrease in band gap as the electron donating spacers were varied from **FL**, to **CBZ**, and **BDT** units (Figure 4).

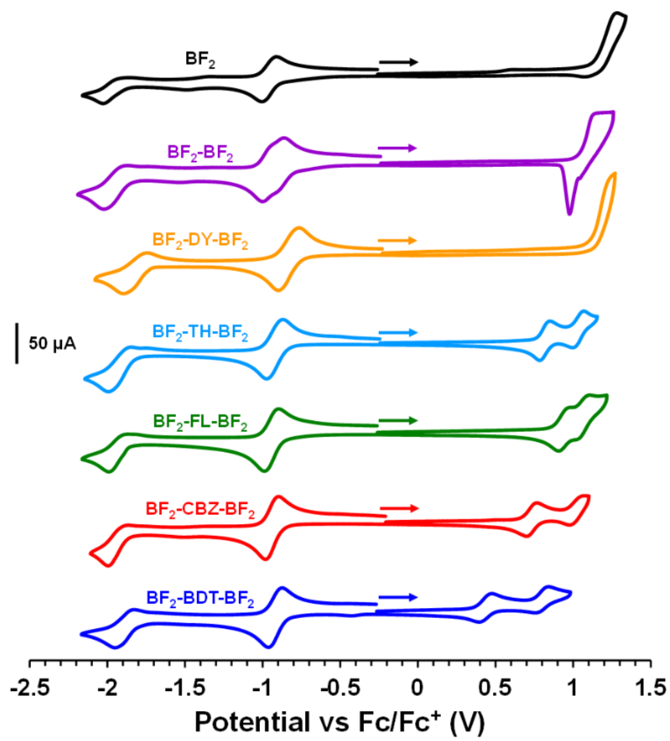

Figure 3. Cyclic voltammograms recorded at 250 mV s^{-1} in 1 mM CH_2Cl_2 solutions containing 0.1 M [*n*Bu_4N][PF_6] as the supporting electrolyte. The scan direction is denoted by the arrows.

Table 2. Solution Phase Cyclic Voltammetry Data Obtained in CH_2Cl_2.[a]

	E_{red2} (V)[b]	E_{red1} (V)	E_{onset}^{red} (V)	E_{ox1} (V)	E_{ox2} (V)	E_{onset}^{ox} (V)	E_g^{CV} (eV)
BF_2	−1.99	−0.94	−0.86	—	—	1.12	1.98
BF_2-BF_2	−1.93	−0.88, −0.97[c]	−0.77	—	—	1.04	1.81
BF_2-DY-BF_2	−1.82	−0.83	−0.75	—	—	1.12	1.87
BF_2-TH-BF_2	−1.96	−0.90	−0.84	0.82	1.07	0.76	1.60
BF_2-FL-BF_2	−1.98	−0.93	−0.85	1.01	1.13	0.86	1.71
BF_2-CBZ-BF_2	−1.99	−0.94	−0.86	0.72	1.06	0.67	1.53
BF_2-BDT-BF_2	−1.90	−0.89	−0.84	0.46	0.86	0.37	1.21

[a]Potentials reported relative to the Fc/Fc^+ redox couple. [b]Irreversible wave, potentials are reported at maximum cathodic current. [c]E_{red1} is split into two overlapping waves.

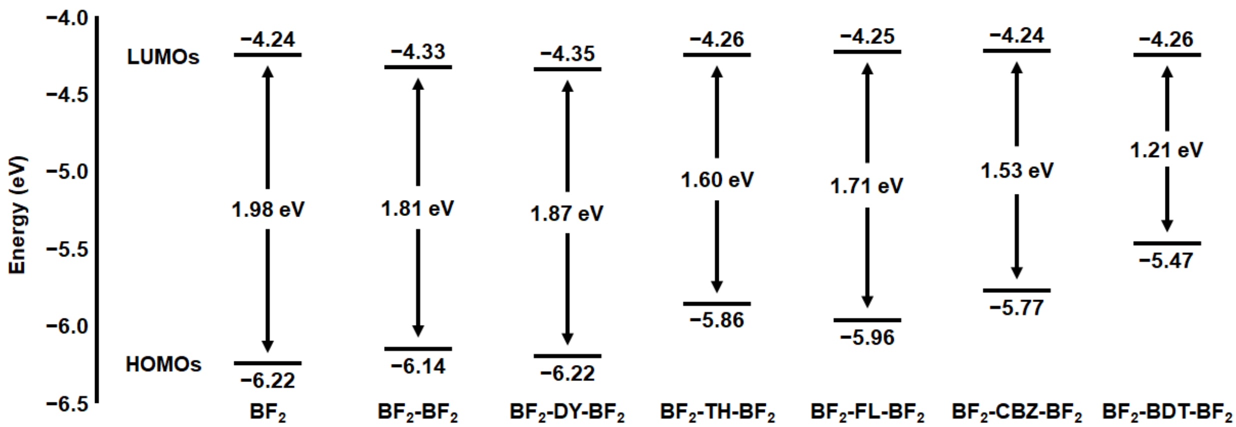

Figure 4. HOMO and LUMO energies estimated from cyclic voltammograms. $E_{LUMO} = -5.1 - E_{onset}^{red}$. $E_{HOMO} = -5.1 - E_{onset}^{ox}$. $E_g^{CV} = E_{LUMO} - E_{HOMO}$.

CONCLUSIONS

This work has led to a demonstration and understanding of the optoelectronic properties of a series of A-D-A compounds incorporating electron accepting BF_2 formazanates bridged by π-conjugated spacers with different π-electron counts and donor characteristics. Theoretical calculations implicate the HOMO and LUMO as the dominant orbital pair associated with the low-energy absorption bands. All compounds exhibited absorption properties (λ_{max} = 509 to 596 nm in CH_2Cl_2 and 528 nm to 645 nm as thin films), and thus E_g^{Opt}, that were tunable by the choice of π-conjugated spacer. In general, a decrease in E_g^{Opt} was observed as the size of π-electron system was increased from monomeric compound **BF_2** (1.89 eV) to A-D-A compounds (*e.g.*, 1.39 eV for **BF_2-BDT-BF_2**), although the planarity of the A-D-A π systems was also an important factor.

The formazanate-based reduction waves corresponding to the formation of radical anions and dianions in the respective CVs exhibited similar reduction potentials (and LUMO energies), allowing us to conclude that they are primarily centered on the BF_2 formazanate units, as implied by DFT calculations. When electron-rich spacers such as TH, FL, CBZ, and BDT were conjugated to BF_2 formazanates, two reversible oxidation waves corresponding to the formation of radical cations and dications were also observed. The oxidation potentials (and HOMO energies) were controlled by the size and electron-donating traits of the bridging spacers. In this series, **BF_2-BDT-BF_2** has the largest π-electron system, and thus it exhibits the lowest oxidation potential and highest HOMO energy. By tuning the HOMO energies, we were able to control the E_g^{CV} of these molecules. A decrease in E_g^{CV} was observed from 1.98 eV for monomeric compound **BF_2** to 1.71 eV for **BF_2-FL-BF_2**, 1.53 eV for **BF_2-CBZ-BF_2**, and 1.21 eV for **BF_2-BDT-BF_2**.

In conclusion, we have shown that the band gaps of A-D-A BF_2 formazanates can be rationally tuned through variation of the bridging donor species and that the combination of BF_2 formazanates and alkoxylated BDT donors are ideal for the creation of low band-gap materials. A-D-A BF_2 formazanates offer narrower band gaps and are generally easier to synthesize than similar systems based on boron dipyrromethene (BODIPY) and related acceptors.[15c, 37] In executing this work, we have created new materials and design strategies for use in the organic electronics arena.

EXPERIMENTAL SECTION

General Considerations

Reactions and manipulations were carried out under a N_2 atmosphere using standard Schlenk techniques unless otherwise stated. Solvents were obtained from Caledon Laboratories, dried using an Innovative Technologies Inc. solvent purification system, collected under vacuum and stored under a N_2 atmosphere over 4 Å molecular sieves. Reagents were purchased from Sigma-Aldrich, Oakwood Chemicals, or TCI America and used as received. **BF_2**,[27] **BF_2-DY-BF_2**,[19a] 2,7-bis(trimethylstannyl)-9,9-dihexylfluorene,[38] and 3,6-dibromo-9-(2-ethylhexyl)-9H-carbazole[39] were prepared according to literature procedures. Stille cross-coupling reactions were run in sealed pressure tubes using an Anton Paar Monowave 50 reactor.

NMR spectra were recorded on 400 MHz (^{1}H: 399.8 MHz, ^{13}C{^{1}H}: 100.6 MHz, ^{11}B: 128.3 MHz, ^{19}F{^{1}H}: 376.1 MHz, ^{119}Sn: 149.1 MHz) Bruker AvanceIII HD or 600 MHz (^{13}C{^{1}H}: 150.7 MHz) Varian INOVA instruments. ^{1}H NMR spectra were referenced to residual $CHCl_3$ (7.26 ppm) and ^{13}C{^{1}H} NMR spectra were referenced to $CDCl_3$ (77.2 ppm). ^{11}B NMR spectra were referenced to $BF_3{\cdot}OEt_2$ (0 ppm), ^{19}F NMR spectra were referenced to $CFCl_3$ (0 ppm), and ^{119}Sn NMR spectra were referenced to $SnMe_4$ (0 ppm). Mass spectra were recorded in positive-ion mode using a Agilent 1969 ToF mass spectrometer using electrospray ionization at McMaster University. FT-IR spectra were recorded on a PerkinElmer Spectrum Two instrument using an attenuated total reflectance accessory. UV-vis absorption spectra were recorded using a Cary 5000 UV-Vis-NIR spectrophotometers scanning from 200 nm to 1500 nm. In solution, four separate concentrations were run for each sample and molar extinction coefficients were determined from the slope of a plot of absorbance against concentration. Emission spectra were obtained using a Photon Technology International (PTI) QM-4 SE spectrofluorometer. Excitation wavelengths were chosen based on the lowest energy absorption maximum from the respective UV-Vis absorption spectrum of each compound.

Electrochemical Methods

Cyclic voltammetry experiments were performed with a Bioanalytical Systems Inc. (BASi) Epsilon potentiostat and analyzed using BASi Epsilon software. Electrochemical cells consisted of a three-electrode setup including a glassy carbon working electrode, platinum wire counter electrode and silver wire *pseudo* reference electrode. Experiments were run at a scan rate of 250 mV s^{-1} in degassed CH_2Cl_2 solutions of the analyte (~1 mM) and supporting electrolyte (0.1 M [$n$$Bu_4N$][$PF_6$]). Cyclic voltammograms were referenced against an internal standard (~1 mM ferrocene) and corrected for internal cell resistance using the BASi Epsilon software.

Thin Film Preparation

Thin films were prepared by filtering (PTFE membrane, 0.22 µm) approximately 100 µL of a 10 mg mL^{-1} solution in $CHCl_3$ directly onto a stationary quartz slide. The sample was then accelerated at a rate of 200 rpm s^{-1} to 2000 rpm and spun for 30 s.

Computational Methods

Electronic structure calculations were performed using the Gaussian 16 software package[40] on a local machine and through the Graham cluster of Compute Canada. Calculations were carried out using the DGDZVP2 basis set and PBE0[34] and LC-ωhPBE[32] density functionals with a tuned value of the range separation parameter ω=0.14 and the polarizable continuum model (PCM) of implicit solvation. The ground-state geometries of these compounds were found by exploring various initial conformations and choosing those with lowest energy. The lowest-energy LC-ωhPBE(ω=0.14)/DGDZVP2 and PBE0/DGDZVP2 structures of all compounds were explicitly confirmed by vibrational analysis to be true minima in all cases. TDDFT excitation energies of all compounds were calculated using nonequilibrium solvation models.

Synthetic Procedures

Synthesis of Fz-Br

In air, phenylhydrazine (0.940 g, 8.72 mmol) was dissolved in absolute EtOH (15 mL). Benzaldehyde (0.920 g, 8.72 mmol) was then added and the solution was stirred for 10 min. After this time, a light yellow precipitate had formed. CH_2Cl_2 (50 mL) and deionized H_2O (50 mL) were added to form a biphasic reaction mixture. Na_2CO_3 (2.96 g, 27.9 mmol) and [$n$$Bu_4N$][Br] (0.28 g, 0.087 mmol) were added and the mixture was cooled with stirring to 0 °C. In a separate flask, 4-bromoaniline (1.50 g, 8.72 mmol) was suspended in deionized H_2O (15 mL) and cooled to 0 °C. To this solution, concentrated HCl (2.25 mL, 26.1 mmol) was added. A cooled solution of $NaNO_2$ (0.692 g, 10.0 mmol) in H_2O (5 mL) was added slowly to the aniline solution over a 15 min period. The mixture was stirred at 0 °C for a further 20 min before it was added dropwise to the biphasic hydrazone-containing reaction mixture described above over a 10 min period. The resulting solution was stirred at 0 °C for 4 h, gradually turning dark red over this period. The organics were extracted into CH_2Cl_2 and the resulting solution was washed with deionized H_2O (3 × 50 mL), dried over anhydrous $MgSO_4$, gravity filtered and concentrated *in vacuo*. The resulting residue was purified by column chromatography (CH_2Cl_2, 100 mL dry neutral alumina, 2.0″ diameter column, R_f = 0.95), concentrated *in vacuo*, and then triturated with cold MeOH to afford **Fz-Br** as a dark red solid. Yield = 2.4 g, 73%. ^{1}H NMR (399.8 MHz, $CDCl_3$): δ 15.35 (s, 1H, N*H*), 8.12 (d, 2H, $^3J_{HH}$ = 8 Hz, aryl C*H*), 7.71 (d, 2H, $^3J_{HH}$ = 8 Hz, aryl C*H*), 7.58−7.53 (m, 4H, aryl C*H*), 7.46 (q, 4H, $^3J_{HH}$ = 8 Hz, aryl C*H*), 7.38–7.30 (m, 2H, aryl C*H*). ^{13}C{^{1}H} NMR (150.7 MHz, $CDCl_3$): δ 148.2, 146.7, 141.5, 137.3, 132.7, 129.6, 128.6, 128.2, 128.0, 126.0, 120.5, 120.0, 119.3. FT-IR

(ATR): 2961 (m), 2924 (s), 2854 (m), 1596 (w), 1505 (m), 1488 (m), 1404 (w), 1350 (w), 1232 (m), 1188 (w), 1068 (w), 1044 (w), 1019 (w), 828 (w), 764 (m), 691 (m) cm^{-1}. Mass Spec. (ESI, +ve mode): exact mass calculated for $[C_{19}H_{15}BrN_4 + H]^+$: 379.0558; exact mass found: 379.0547; difference: −2.9 ppm.

Synthesis of BF_2-Br

Formazan **Fz-Br** (1.45 g, 3.80 mmol) was dissolved in dry toluene (100 mL). NEt_3 (1.16 g, 1.60 mL, 11.5 mmol) was then added, followed by the dropwise addition of $BF_3{\cdot}OEt_2$ (2.72 g, 2.40 mL, 19.1 mmol). The reaction mixture was heated to reflux for 16 h during which the colour changed from dark red to deep purple. The solution was then cooled to room temperature and the remaining reactive boron-containing species were quenched with H_2O (10 mL). The purple toluene solution was washed with H_2O (3 × 100 mL), dried over anhydrous $MgSO_4$, gravity filtered and concentrated *in vacuo*. The resulting residue was purified by column chromatography (CH_2Cl_2, 100 mL dry neutral alumina, 2.0″ diameter column, R_f = 0.90), concentrated *in vacuo*, and then triturated with cold MeOH to afford **BF_2-Br** as a dark purple solid. Yield = 0.90 g, 55%. ^{1}H NMR (399.8 MHz, $CDCl_3$): δ 8.10 (dd, 2H, $^3J_{HH}$ = 8 Hz, $^3J_{HH}$ = 2 Hz, aryl C*H*), 7.93 (d, 2H, $^3J_{HH}$ = 8 Hz, aryl C*H*), 7.80 (d, 2H, $^3J_{HH}$ = 8 Hz, aryl C*H*), 7.61 (d, 2H, $^3J_{HH}$ = 8 Hz, aryl C*H*), 7.53−7.43 (m, 6H, aryl C*H*). ^{11}B NMR (128.3 MHz, $CDCl_3$): δ –0.6 (t, $^1J_{BF}$ = 29 Hz). ^{13}C{^{1}H} NMR (150.7 MHz, $CDCl_3$): δ 149.3, 144.0, 142.9, 133.5, 132.4, 130.2, 129.6, 129.3, 128.9, 125.6, 124.8, 124.0, 123.6. ^{19}F{^{1}H} NMR (376.1 Hz, $CDCl_3$): δ –143.8 (q, $^1J_{FB}$ = 29 Hz). FT-IR (ATR): 3067 (w), 2964 (w), 2924 (m), 2854 (w), 1582 (w), 1484 (m), 1464 (w), 1352 (m), 1297 (s), 1268 (s), 1175 (w), 1117 (m), 1074 (w), 1026 (m), 1006 (w), 966 (m) 827 (w), 764 (m), 691 (w) cm^{-1}. Mass Spec. (ESI, +ve mode): exact mass calculated for $[C_{19}H_{14}BBrF_2N_4 + H]^+$: 427.0541; exact mass found: 427.0556; difference: +3.5 ppm.

Synthesis of 9-(2-ethylhexyl)-3,6-bis(trimethylstannyl)-9H-carbazole (Me_3Sn-CBZ-$SnMe_3$)

According to an adapted literature procedure,[41] a solution of 3,6-dibromo-9-(2-ethylhexyl)-carbazole (0.55 g, 1.3 mmol) in dry THF (25 mL) was cooled to −78 °C for 10 min, followed by the dropwise addition of 2.5 M *n*-butyllithium in hexanes (1.1 mL, 2.8 mmol). The resulting solution was stirred at −78 °C for 1 h. In a separate Schlenk flask, a solution of trimethyltin chloride (0.63 g, 3.1 mmol) in dry THF (3 mL) was prepared and added to the bright-yellow lithium-containing mixture in one-portion. The resulting colourless solution was gradually warmed to room temperature and stirred for 12 h. The reaction was diluted with Et_2O (50 mL), washed with H_2O (50 mL), sat. $NaHCO_3$ (2 × 50 mL), H_2O (50 mL), dried over anhydrous $MgSO_4$, gravity filtered and concentrated *in vacuo* to give the crude product as a light-yellow oil. The crude oil was used for Stille cross-coupling reaction without further purification. Yield = 0.60 g, 79%. ^{1}H NMR (399.8 MHz, $CDCl_3$): Selected assigned signals: δ 8.33 (s, 2H, aryl C*H*), 7.62 (d, 2H, $^3J_{HH}$ = 8 Hz, aryl C*H*), 7.46 (d, 2H, $^3J_{HH}$ = 8 Hz, aryl C*H*), 4.24−4.13 (m, 2H, NCH_2), 2.16−2.09 (m, 1H, NCH_2C*H*), 0.99−0.94 (m, 9H, Alkyl C*H*), 0.45 (s, 18H, Sn(CH_3)3). ^{119}Sn NMR (149.1 MHz, $CDCl_3$): δ −23.4 (s).

General Procedure for Stille Cross-Coupling Reactions in a Anton Paar Monowave 50 Reactor

Mono-bromo substituted BF_2 formazanate **BF_2-Br** (2 equiv.), bis-trimethyltin reagent (1 equiv.), $Pd_2(dba)_3$ (5 mol %), and P(*o*-tol)$_3$ (10 mol %) were added to oven dried 10 mL glass pressure tubes. The tubes were equipped with a rubber septum and purged using three evacuation/fill cycles, followed by addition of dry, degassed toluene. The tubes were then sealed and heated in an Anton Paar Monowave 50 reactor under the following conditions: i) ramp temperature to 170 °C over 8 min, ii) hold temperature at 170 °C for 15 min. Pressures were maintained at approximately 4 bar during this time. After the 15 min reaction time, the mixtures were allowed to cool to room temperature and volatiles were removed *in vacuo* to afford crude mixtures.

Synthesis of BF_2-BF_2

From **BF_2-Br** (0.094 g, 0. 22 mmol), hexamethylditin (0.036 g, 0.11 mmol), $Pd_2(dba)_3$ (0.005 g, 0.005 mmol), P(*o*-tol)$_3$ (0.005 g, 0.011 mmol) in 4 mL toluene. The maximum pressure reached was 3.5 bar. The crude reaction products were purified by column chromatography (gradient 1:2 to 1:1 CH_2Cl_2:hexanes (v/v), 250 mL dry silica, 2.0″ diameter column, R_f = 0.10) to afford the **BF_2-BF_2** complex as a dark purple film. The film was redissolved in minimal CH_2Cl_2 (4 mL) and precipitated into a large excess of cold pentane (–20 °C, 40 mL) with vigorous stirring. The solids were isolated by vacuum filtration to afford the **BF_2-BF_2** as a dark purple solid. Yield = 0.022 g, 29%. ^{1}H NMR (399.8 MHz, $CDCl_3$): δ 8.14 (d, 4H, $^3J_{HH}$ = 7 Hz, aryl C*H*), 8.04 (d, 4H, $^3J_{HH}$ = 8 Hz, aryl C*H*), 7.94 (d, 4H, $^3J_{HH}$ = 8 Hz, aryl C*H*), 7.76 (d, 4H, $^3J_{HH}$ = 8 Hz, aryl C*H*), 7.52–7.44 (m, 12H, aryl C*H*). ^{11}B NMR (128.3 MHz, $CDCl_3$): δ –0.5 (t, $^1J_{BF}$ = 29 Hz). ^{13}C{^{1}H} NMR (100.6 MHz, $CDCl_3$): δ 149.4, 144.0, 143.8, 141.0, 133.7, 130.0, 129.5, 129.3, 128.9, 127.9, 125.7, 124.1, 123.6. ^{19}F{^{1}H} NMR (376.1 Hz, $CDCl_3$): δ –143.8 (q, $^1J_{FB}$ = 29 Hz). FT-IR (ATR): 3074 (w), 3038 (w), 1601 (m), 1492 (w), 1352 (m), 1293 (s), 1268 (s), 1222 (m), 1180 (w), 1025 (m), 964 (s), 762 (s), 690 (m) cm^{-1}. UV-vis (CH_2Cl_2): λ_{max} 570 nm (ε = 47,300 M^{-1} cm^{-1}), 313 nm (ε = 34,000 M^{-1} cm^{-1}), 261 nm (ε = 28,100 M^{-1} cm^{-1}). Mass Spec. (ESI, +ve mode): exact mass calculated for $[C_{38}H_{28}B_2F_4N_8 + H]^+$: 695.2637; exact mass found: 695.2640; difference: +0.4 ppm.

Synthesis of BF_2-TH-BF_2

From **BF_2-Br** (0.075 g, 0.176 mmol), 2,5-bis(trimethylstannyl) thiophene (0.036 g, 0.088 mmol), $Pd_2(dba)_3$ (0.004 g, 0.004 mmol), P(*o*-tol)$_3$ (0.003 g, 0.009 mmol) in 6 mL toluene. The maximum pressure reached was 4.8 bar. The crude reaction products were purified by column chromatography (gradient 1:2 to 1:1 toluene:hexanes (v/v), 300 mL dry silica, 2.0″ diameter column, R_f = 0.10) to afford **BF_2-TH-BF_2** complex as a dark blue film. The film was redissolved in minimal CH_2Cl_2 (3 mL) and precipitated into a large excess of cold pentane (–20 °C, 30 mL) with vigorous stirring. The solids were isolated by vacuum filtration to afford **BF_2-TH-BF_2** as a dark blue solid. Yield = 0.084 g, 74%. ^{1}H NMR (399.8 MHz, $CDCl_3$): δ 8.13 (d, 4H, $^3J_{HH}$ = 8 Hz, aryl C*H*), 7.99 (d, 4H, $^3J_{HH}$ = 8 Hz, aryl C*H*), 7.93 (d, 4H, $^3J_{HH}$ = 8 Hz, aryl C*H*), 7.74 (d, 4H, $^3J_{HH}$ = 8 Hz, aryl C*H*), 7.52–7.45 (m, 12H, aryl C*H*), 7.43 (s, 2H, thiophene C*H*). ^{11}B NMR (128.3 MHz, $CDCl_3$): δ –0.5 (t, $^1J_{BF}$ = 29 Hz). ^{13}C{^{1}H} NMR (150.7 MHz, $CDCl_3$): δ 149.2, 144.1, 143.7, 143.4, 135.4, 133.8, 129.9, 129.5, 129.3, 128.9, 126.2, 125.8, 125.7, 124.1, 123.6. ^{19}F{^{1}H} NMR (376.1 Hz, $CDCl_3$): δ –143.7 (q, $^1J_{FB}$ = 29 Hz). FT-IR (ATR): 3069 (w), 2964 (m), 2923 (s), 2854 (m), 1596 (m), 1350 (w), 1297 (s), 1268 (s), 1179 (w), 1025 (w), 969 (m), 763 (s), 751 (s) cm^{-1}. UV-vis (CH_2Cl_2): λ_{max} 596 nm (ε = 52,400 M^{-1} cm^{-1}), 316 nm (ε = 29,500 M^{-1} cm^{-1}), 294 nm (ε = 27,300 M^{-1} cm^{-1}), 265 nm (ε = 22,900 M^{-1} cm^{-1}). Mass Spec. (ESI, +ve mode): exact mass calculated for $[C_{42}H_{30}B_2F_4N_8S + H]^+$: 777.2515; exact mass found: 777.2511; difference: −0.5 ppm.

Synthesis of BF_2-FL-BF_2

From **BF_2-Br** (0.074 g, 0.173 mmol), 2,7-bis(trimethylstannyl)-9,9-dihexylfluorene (0.057 g, 0.086 mmol), $Pd_2(dba)_3$ (0.004 g, 0.004 mmol), P(*o*-tol)$_3$ (0.003 g, 0.009 mmol) in 5 mL toluene. The maximum pressure reached was 4.1 bar. The crude reaction products were purified by column chromatography (gradient 1:2 to 1:1 toluene:hexanes (v/v), 300 mL dry silica, 2.0″ diameter column, R_f = 0.10) to afford **BF_2-FL-BF_2** complex as a dark purple film. The film was redissolved in minimal CH_2Cl_2 (4 mL) and precipitated into a large excess of cold pentane (–20 °C, 40 mL) with vigorous stirring. The solids were isolated by vacuum filtration to afford **BF_2-FL-BF_2** as a dark purple solid. Yield = 0.042 g, 49%. ^{1}H NMR (399.8 MHz, $CDCl_3$): δ 8.15 (d, 4H, $^{3}J_{HH}$ = 8 Hz, aryl C*H*), 8.05 (d, 4H, $^{3}J_{HH}$ = 8 Hz, aryl C*H*), 7.94 (d, 4H, $^{3}J_{HH}$ = 8 Hz, aryl C*H*), 7.83–7.79 (m, 6H, aryl C*H*), 7.65 (d, 2H, $^{3}J_{HH}$ = 8 Hz, aryl C*H*), 7.61 (br s, 2H, aryl C*H*), 7.53–7.43 (m, 12H, aryl C*H*), 2.08–2.04 (m, 4H, CH_2), 1.14–1.04 (m, 12H, CH_2), 0.77–0.72 (m, 10H, overlapping CH_2 and CH_3). ^{11}B NMR (128.3 MHz, $CDCl_3$): δ –0.4 (t, $^{1}J_{BF}$ = 29 Hz). ^{13}C{^{1}H} NMR (150.7 MHz, $CDCl_3$): δ 152.2, 149.1, 144.1, 143.1, 140.8, 139.0, 133.8, 129.8, 129.5, 129.3, 128.9, 127.9, 126.4, 125.7, 124.0, 123.6, 121.7, 120.6, 55.6, 40.5, 31.6, 29.8, 24.0, 22.7, 14.1. ^{19}F{^{1}H} NMR (376.1 Hz, $CDCl_3$): δ –143.9 (q, $^{1}J_{FB}$ = 29 Hz). FT-IR (ATR): 3075 (w), 2957 (m), 2924 (s), 2854 (m), 1598 (m), 1466 (m), 1351 (w), 1296 (s), 1270 (s), 1222 (w), 1180 (w), 1026 (w), 969 (m), 763 (m), 691 (m) cm^{-1}. UV-vis (CH_2Cl_2): λ_{max} 560 nm (ε = 58,200 M^{-1} cm^{-1}), 320 nm (ε = 55,400 M^{-1} cm^{-1}). Mass Spec. (ESI, +ve mode): exact mass calculated for $[C_{63}H_{60}B_2F_4N_8 + H]^+$: 1027.5141; exact mass found: 1027.5124; difference: −1.7 ppm.

Synthesis of BF_2-CBZ-BF_2

From **BF_2-Br** (0.089 g, 0. 207 mmol), 9-(2-ethylhexyl)-3,6-bis(trimethylstannyl)-9H-carbazole (0.063 g, 0.104 mmol), $Pd_2(dba)_3$ (0.005 g, 0.005 mmol), P(*o*-tol)$_3$ (0.003 g, 0.010 mmol) in 5 mL toluene. The maximum pressure reached was 3.3 bar. The crude reaction products were purified by column chromatography (gradient 1:2 to 1:1 CH_2Cl_2:hexanes (v/v), 350 mL dry silica, 2.0″ diameter column, R_f = 0.10) to afford **BF_2-CBZ-BF_2** complex as a dark purple film. The film was redissolved in minimal CH_2Cl_2 (3 mL) and precipitated into a large excess of cold pentane (–20 °C, 30 mL) with vigorous stirring. The solids were isolated by vacuum filtration to afford **BF_2-CBZ-BF_2** as a dark purple solid. Yield = 0.048 g, 48%. ^{1}H NMR (399.8 MHz, $CDCl_3$): δ 8.46 (s, 2H, aryl C*H*), 8.20 (d, 4H, $^{3}J_{HH}$ = 8 Hz, aryl C*H*), 8.09 (d, 4H, $^{3}J_{HH}$ = 8 Hz, aryl C*H*), 7.98 (d, 4H, $^{3}J_{HH}$ = 8 Hz, aryl C*H*), 7.88 (d, 4H, $^{3}J_{HH}$ = 8 Hz, aryl C*H*), 7.81 (d, 2H, $^{3}J_{HH}$ = 8 Hz, aryl C*H*), 7.53–7.45 (m, 14H, aryl C*H*), 4.24 (br s, 2H, N-CH_2), 2.14 (br s, 1H, C*H*), 1.46–1.30 (m, 8H, CH_2), 0.98 (t, 3H, $^3J_{HH}$ = 7 Hz, CH_3), 0.92 (t, 3H, $^3J_{HH}$ = 7 Hz, CH_3). ^{11}B NMR (128.3 MHz, $CDCl_3$): δ –0.4 (t, $^1J_{BF}$ = 29 Hz). ^{13}C{^{1}H} NMR (150.7 MHz, $CDCl_3$): δ 149.2, 144.1, 143.6, 142.6, 141.5, 133.9, 131.1, 129.7, 129.4, 129.2, 128.9, 127.7, 125.7, 125.5, 124.0, 123.7, 123.5, 119.2, 109.9, 47.8, 39.6, 31.2, 29.0, 24.5, 23.2, 14.2, 11.1. ^{19}F{^{1}H} NMR (376.1 Hz, $CDCl_3$): δ –144.0 (q, $^1J_{FB}$ = 29 Hz). FT-IR (ATR): 3069 (w), 2957 (m), 2925 (s), 2854 (m), 1593 (m), 1481 (m), 1465 (m), 1354 (w), 1294 (s), 1270 (s), 1222 (w), 1180 (w), 1025 (w), 968 (m), 760 (m), 690 (m) cm^{-1}. UV-vis (CH_2Cl_2): λ_{max} 563 nm (ε = 46,400 M^{-1} cm^{-1}), 307 nm (ε = 50,800 M^{-1} cm^{-1}). Mass Spec. (ESI, +ve mode): exact mass calculated for [$C_{58}H_{51}B_2F_4N_9$ + H]$^+$: 972.4468; exact mass found: 972.4478; difference: +1.0 ppm.

Synthesis of BF$_2$-BDT-BF$_2$

From **BF$_2$-Br** (0.035 g, 0.082 mmol), 2,6-Bis(trimethylstannyl)-4,8-bis(2-ethylhexyloxy) benzo[1,2-b:4,5-b′]dithiophene (0.032 g, 0.041 mmol), $Pd_2(dba)_3$ (0.002 g, 0.002 mmol), P(*o*-tol)$_3$ (0.002 g, 0.004 mmol) in 5 mL toluene. The maximum pressure reached was 3.9 bar. The crude reaction products were purified by column chromatography (gradient 1:2 to 1:1 CH_2Cl_2:hexanes (v/v), 350 mL dry silica, 2.0″ diameter column, R_f = 0.10) to afford **BF$_2$-BDT-BF$_2$** complex as a dark blue film. The film was redissolved in minimal CH_2Cl_2 (2 mL) and precipitated into a large excess of cold pentane (–20 °C, 20 mL) with vigorous stirring. The solids were isolated by vacuum filtration to afford **BF$_2$-BDT-BF$_2$** as a dark blue solid. Yield = 0.033 g, 70%. ^{1}H NMR (399.8 MHz, $CDCl_3$): δ 8.14 (d, 4H, $^3J_{HH}$ = 8 Hz, aryl C*H*), 8.01 (d, 4H, $^3J_{HH}$ = 8 Hz, aryl C*H*), 7.97 (d, 4H, $^3J_{HH}$ = 8 Hz, aryl C*H*), 7.81 (d, 4H, $^3J_{HH}$ = 8 Hz, aryl C*H*), 7.74 (s, 2H, thiophene C*H*), 7.52–7.45 (m, 12H, aryl C*H*), 4.24 (d, 4H, $^3J_{HH}$ = 5 Hz, O-CH_2), 1.91–1.86 (m, 2H, C*H*), 1.80–1.73 (m, 2H, CH_2), 1.71–1.63 (m, 4H, CH_2), 1.61–1.56 (m, 2H, CH_2), 1.51–1.42 (m, 8H, CH_2), 1.09 (t, 6H, $^3J_{HH}$ = 7 Hz, CH_3), 1.00 (t, 6H, $^3J_{HH}$ = 7 Hz, CH_3). ^{11}B NMR (128.3 MHz, $CDCl_3$): δ –0.5 (t, $^1J_{BF}$ = 29 Hz). ^{13}C{^{1}H} NMR (150.7 MHz, $CDCl_3$): δ 149.1, 144.8, 144.1, 143.8, 142.4, 135.5, 133.8, 133.2, 130.0, 129.8, 129.5, 129.3, 128.9, 127.0, 125.6, 123.9, 123.5, 117.3, 76.3, 40.9, 30.6, 29.4, 24.0, 23.3, 14.4, 11.5. ^{19}F{^{1}H} NMR (376.1 Hz, $CDCl_3$): δ –143.5 (q, $^1J_{FB}$ = 29 Hz). FT-IR (ATR): 3072 (w), 3042 (w), 2961 (m), 2925 (s), 2856 (m), 1595 (m), 1539 (w), 1455 (m), 1378 (m), 1304 (s), 1267 (s), 1183 (m), 1114 (m), 969 (s), 690 (m) cm^{-1}. UV-vis (CH_2Cl_2): λ_{max} 592 nm (ε = 51,700 M^{-1} cm^{-1}), 371 nm (ε = 34,400 M^{-1} cm^{-1}), 321 nm (ε = 34,100 M^{-1} cm^{-1}), 296 nm (ε = 39,100 M^{-1} cm^{-1}). Mass Spec. (ESI, +ve mode): exact mass calculated for $[C_{64}H_{64}B_2F_4N_8O_2S_2 + H]^+$: 1139.4794; exact mass found: 1139.4786; difference: −0.7 ppm.

ASSOCIATED CONTENT

Supporting Information

The supporting information is available free of charge at #################.

Additional computational data and copies of ^{1}H, ^{11}B, ^{13}C{^{1}H}, and ^{19}F NMR spectra for all compounds.

AUTHOR INFORMATION

Corresponding Author

Joe B. Gilroy – Department of Chemistry and the Centre for Advanced Materials and Biomaterials Research (CAMBR), The University of Western Ontario, London, ON, N6A 5B7, Canada.

orcid.org/0000-0003-0349-7780

E-mail: joe.gilroy@uwo.ca

Authors

Jasveer S. Dhindsa – Department of Chemistry and the Centre for Advanced Materials and Biomaterials Research (CAMBR), The University of Western Ontario, London, ON, N6A 5B7, Canada.

Francis L. Buguis – Department of Chemistry and the Centre for Advanced Materials and Biomaterials Research (CAMBR), The University of Western Ontario, London, ON, N6A 5B7, Canada.

Michael Anghel – Department of Chemistry and the Centre for Advanced Materials and Biomaterials Research (CAMBR), The University of Western Ontario, London, ON, N6A 5B7, Canada.

Notes

The authors declare no competing financial interest.

ACKNOWLEDGEMENTS

This work was supported by the Natural Sciences and Engineering Research Council (NSERC) of Canada (J.S.D. and F.L.B: CGS-D Scholarships; J.B.G.: DG, RGPIN-2018-04240), the Ontario Ministry of Research and Innovation (J.B.G.: ERA, ER-14-10-147), and the Canadian Foundation for Innovation (J.B.G.: JELF, 33977). We would like to thank the facilities of Compute/Calcul Canada for allowing us to run theoretical calculations. We also thank the technical staff at the McMaster Regional Centre for Mass Spectrometry for their thorough approach to analyzing the compounds reported.

REFERENCES

(1) Quinn, J. T. E.; Zhu, J.; Li, X.; Wang, J.; Li, Y. Recent Progress in the Development of n-Type Organic Semiconductors for Organic Field Effect Transistors. *J. Mater. Chem. C* **2017**, *5*, 8654−8681.

(2) Shahnawaz; Swayamprabha, S. S.; Nagar, M. R.; Yadav, R. A. K.; Gull, S.; Dubey, D. K.; Jou, J.-H. Hole-Transporting Materials for Organic Light-Emitting Diodes: An Overview. *J. Mater. Chem. C* **2019**, *7*, 7144−7158.

(3) Kan, B.; Kan, Y.; Zuo, L.; Shi, X.; Gao, K. Recent Progress on All-Small Molecule Organic Solar Cells Using Small-Molecule Nonfullerene Acceptors. *InfoMat* **2021**, *3*, 175–200.

(4) In this study, we use the terms "band gap" and "HOMO-LUMO gap" interchangeably.

(5) Bronstein, H.; Nielsen, C. B.; Schroeder, B. C.; McCulloch, I. The Role of Chemical Design in the Performance of Organic Semiconductors. *Nat. Rev. Chem.* **2020**, *4*, 66−77.

(6) (a) Xiao, S.; Zhang, Q.; You, W. Molecular Engineering of Conjugated Polymers for Solar Cells: An Updated Report. *Adv. Mater.* **2017**, *29*, 1601391; (b) Revoju, S.; Matuhina, A.; Canil, L.; Salonen, H.; Hiltunen, A.; Abate, A.; Vivo, P. Structure-Induced Optoelectronic Properties of Phenothiazine-Based Materials. *J. Mater. Chem. C* **2020**, *8*, 15486−15506.

(7) (a) Yang, Y.; Liu, F.; Wang, H.; Bo, S.; Liu, J.; Qiu, L.; Zhen, Z.; Liu, X. Enhanced Electro-Optic Activity from the Triarylaminophenyl-Based Chromophores by Introducing Heteroatoms to the Donor. *J. Mater. Chem. C* **2015**, *3*, 5297−5306; (b) Xu, H.; Yang, D.; Liu, F.; Fu, M.; Bo, S.; Liu, X.; Cao, Y. Nonlinear Optical Chromophores Based on Dewar's Rules: Enhancement of Electro-Optic Activity by Introducing Heteroatoms into the Donor or Bridge. *Phys. Chem. Chem. Phys.* **2015**, *17*, 29679−29688; (c) Zhang, H.; Iqbal, Z.; Chen, Z.-E.; Hong, Y. Effects of Various Heteroatom Donor Species on the Photophysical, Electrochemical and Photovoltaic Performance

of Dye-Sensitized Solar Cells. *Electrochim. Acta* **2018**, *290*, 303−311; (d) Huang, C.; Liao, X.; Gao, K.; Zuo, L.; Lin, F.; Shi, X.; Li, C.-Z.; Liu, H.; Li, X.; Liu, F.; Chen, Y.; Chen, H.; Jen, A. K.-Y. Highly Efficient Organic Solar Cells Based on S,N-Heteroacene Non-Fullerene Acceptors. *Chem. Mater.* **2018**, *30*, 5429−5434.

(8) (a) Kim, T.-D.; Lee, K.-S. D-π-A Conjugated Molecules for Optoelectronic Applications. *Macromol. Rapid Commun.* **2015**, *36*, 943−958; (b) Wang, Z.; Zhu, L.; Shuai, Z.; Wei, Z. A–π–D–π–A Electron-Donating Small Molecules for Solution-Processed Organic Solar Cells: A Review. *Macromol. Rapid Commun.* **2017**, *38*, 1700470.

(9) Wan, X.; Li, C.; Zhang, M.; Chen, Y. Acceptor–Donor–Acceptor Type Molecules for High Performance Organic Photovoltaics – Chemistry and Mechanism. *Chem. Soc. Rev.* **2020**, *49*, 2828–2842.

(10) Huang, Y.; Zhou, W.; Li, X.; Jiang, L.; Song, Y. Highly Broadband NLO Response of Acceptor–Donor–Acceptor Materials with a Planar Conformation. *Mater. Adv.* **2021**, *2*, 2097–2103.

(11) Zampetti, A.; Minotto, A.; Squeo, B. M.; Gregoriou, V. G.; Allard, S.; Scherf, U.; Chochos, C. L.; Cacialli, F. Highly Efficient Solid-State Near-Infrared Organic Light-Emitting Diodes Incorporating A-D-A Dyes Based on *α*,*β*-Unsubstituted "BODIPY" Moieties. *Sci. Rep.* **2017**, *7*, 1611.

(12) Karthik, D.; Jung, Y. H.; Lee, H.; Hwang, S.; Seo, B.-M.; Kim, J.-Y.; Han, C. W.; Kwon, J. H. Acceptor–Donor–Acceptor-Type Orange–Red Thermally Activated Delayed Fluorescence Materials Realizing External Quantum Efficiency Over 30% with Low Efficiency Roll-Off. *Adv. Mater.* **2021**, *33*, 2007724.

(13) Aswathy, P. R.; Sharma, S.; Tripathi, N. P.; Sengupta, S. Regioisomeric BODIPY Benzodithiophene Dyads and Triads with Tunable Red Emission as Ratiometric Temperature and Viscosity Sensors. *Chem. Eur. J.* **2019**, *25*, 14870−14880.

(14) (a) Cai, Y.; Wei, Z.; Song, C.; Tang, C.; Huang, X.; Hu, Q.; Dong, X.; Han, W. Novel Acceptor–Donor–Acceptor Structured Small Molecule-Based Nanoparticles for Highly Efficient Photothermal Therapy. *Chem. Commun.* **2019**, *55*, 8967−8970; (b) He, Z.; Zhao, L.; Zhang, Q.; Chang, M.; Li, C.; Zhang, H.; Lu, Y.; Chen, Y. An Acceptor–Donor–Acceptor Structured Small Molecule for Effective NIR Triggered Dual Phototherapy of Cancer. *Adv. Funct. Mater.* **2020**, *30*, 1910301.

(15) (a) Antwi, B. Y.; Taylor, R. G. D.; Cameron, J.; Owoare, R. B.; Kingsford-Adaboh, R.; Skabara, P. J. Acceptor–Donor–Acceptor Small Molecules Based on Derivatives of 3,4-Ethylenedioxythiophene for Solution Processed Organic Solar Cells. *RSC Adv.* **2016**, *6*, 98797–98803; (b) Huo, Y.; Zhu, J.; Wang, X.-Z.; Yan, C.; Chai, Y.-F.; Chen, Z.-Z.; Zhan, X.; Zhang, H.-L. Small Molecule Donors Based on Benzodithiophene and Diketopyrrolopyrrole Compatible with Both Fullerene and Non-Fullerene Acceptors. *J. Mater. Chem. C* **2018**, *6*, 5843−5848; (c) Tarafdar, G.; Johnson, J. C.; Larson, B. W.; Ramamurthy, P. C. BODIPY Based A-D-A Molecules: Effect of CF_3 Group Substitution at *Meso* Phenyl Group. *Dyes Pigm.* **2020**, *177*, 108289; (d) Lee, E.; Tran, D. K.; Park, J.; Ko, W.; Jenekhe, S. A.; Hwang, Y.-J. Benzodithiophene-Based Wide-Bandgap Small-Molecule Donors for Organic Photovoltaics with Large Open-Circuit Voltages. *Org. Electron.* **2021**, *88*, 105996.

(16) (a) Yan, C.; Barlow, S.; Wang, Z.; Yan, H.; Jen, A. K.-Y.; Marder, S. R.; Zhan, X. Non-Fullerene Acceptors for Organic Solar Cells. *Nat. Rev. Mater.* **2018**, *3*, 18003; (b) Zhang, G.; Zhao, J.; Chow, P. C. Y.; Jiang, K.; Zhang, J.; Zhu, Z.; Zhang, J.; Huang, F.; Yan, H. Nonfullerene

Acceptor Molecules for Bulk Heterojunction Organic Solar Cells. *Chem. Rev.* **2018**, *118*, 3447−3507; (c) Yuan, J.; Zhang, Y.; Zhou, L.; Zhang, G.; Yip, H.-L.; Lau, T.-K.; Lu, X.; Zhu, C.; Peng, H.; Johnson, P. A.; Leclerc, M.; Cao, Y.; Ulanski, J.; Li, Y.; Zou, Y. Single-Junction Organic Solar Cell with Over 15% Efficiency Using Fused-Ring Acceptor with Electron-Deficient Core. *Joule* **2019**, *3*, 1140−1151; (d) Cui, Y.; Yao, H.; Zhang, J.; Xian, K.; Zhang, T.; Hong, L.; Wang, Y.; Xu, Y.; Ma, K.; An, C.; He, C.; Wei, Z.; Gao, F.; Hou, J. Single-Junction Organic Photovoltaic Cells with Approaching 18% Efficiency. *Adv. Mater.* **2020**, *32*, 1908205; (e) Ye, W.; Yang, Y.; Zhang, Z.; Zhu, Y.; Ye, L.; Miao, C.; Lin, Y.; Zhang, S. Nonfullerene All-Small-Molecule Organic Solar Cells: Prospect and Limitation. *Sol. RRL* **2020**, *4*, 2000258; (f) Wang, K.; Chen, J.; Hu, J.; Guo, X.; Zhang, M.; Li, Y. A Small Molecule Acceptor with a Heptacyclic Benzodi(thienocyclopentafuran) Central Unit Achieving 13.4% Efficiency in Polymer Solar Cells with Low Energy Loss. *J. Mater. Chem. C* **2021**, *9*, 2744–2751.

(17) Gilroy, J. B.; Otten, E. Formazanate Coordination Compounds: Synthesis, Reactivity, and Applications. *Chem. Soc. Rev.* **2020**, *49*, 85–113.

(18) (a) Chang, M.-C.; Otten, E. Synthesis and Ligand-Based Reduction Chemistry of Boron Difluoride Complexes with Redox-Active Formazanate Ligands. *Chem. Commun.* **2014**, *50*, 7431−7433; (b) Barbon, S. M.; Price, J. T.; Reinkeluers, P. A.; Gilroy, J. B. Substituent-Dependent Optical and Electrochemical Properties of Triarylformazanate Boron Difluoride Complexes. *Inorg. Chem.* **2014**, *53*, 10585−10593; (c) Maar, R. R.; Barbon, S. M.; Sharma, N.; Groom, H.; Luyt, L. G.; Gilroy, J. B. Evaluation of Anisole-Substituted Boron Difluoride Formazanate Complexes for Fluorescence Cell Imaging. *Chem. Eur. J.* **2015**, *21*, 15589−15599; (d) Chang, M.-C.; Chantzis, A.; Jacquemin, D.; Otten, E. Boron Difluorides with Formazanate Ligands: Redox-Switchable Fluorescent Dyes with Large Stokes Shifts. *Dalton Trans.* **2016**, *45*, 9477–9484.

(19) (a) Dhindsa, J. S.; Maar, R. R.; Barbon, S. M.; Olivia Avilés, M.; Powell, Z. K.; Lagugné-Labarthet, F.; Gilroy, J. B. A π-Conjugated Inorganic Polymer Constructed from Boron Difluoride Formazanates and Platinum(II) Diynes. *Chem. Commun.* **2018**, *54*, 6899−6902; (b) Kumar, C.; Agrawal, A. R.; Ghosh, N. G.; Karmakar, H. S.; Das, S.; Kumar, N. R.; Banewar, V. W.; Zade, S. S. Boron Difluoride Formazanates with Thiophene and 3,4-Ethylenedioxythiophene Capping and Their Electrochemical Polymerization. *Dalton Trans.* **2020**, *49*, 13202−13206; (c) Kawano, Y.; Ito, Y.; Ito, S.; Tanaka, K.; Chujo, Y. π-Conjugated Copolymers Composed of Boron Formazanate and Their Application for a Wavelength Converter to Near-Infrared Light. *Macromolecules* **2021**, *54*, 1934–1942.

(20) Xiang, H.; Zhao, L.; Yu, L.; Chen, H.; Wei, C.; Chen, Y.; Zhao, Y. Self-Assembled Organic Nanomedicine Enables Ultrastable Photo-to-Heat Converting Theranostics in the Second Near-Infrared Biowindow. *Nat. Commun.* **2021**, *12*, 218.

(21) Buguis, F. L.; Maar, R. R.; Staroverov, V. N.; Gilroy, J. B. Near-Infrared Boron Difluoride Formazanate Dyes. *Chem. Eur. J.* **2021**, *27*, 2854–2860.

(22) Hesari, M.; Barbon, S. M.; Mendes, R. B.; Staroverov, V. N.; Ding, Z.; Gilroy, J. B. Structural Tuning of Boron Difluoride Formazanate Electrochemiluminescence Mediated by Tri-n-propylamine. *J. Phys. Chem. C.* **2018**, *122*, 1258−1266.

(23) Barbon, S. M.; Gilroy, J. B. Boron Difluoride Formazanate Copolymers with 9,9-Di-n-hexylfluorene Prepared by Copper-Catalyzed Alkyne-Azide Cycloaddition Chemistry. *Polym. Chem.* **2016**, *7*, 3589−3598.

(24) (a) Chang, M.-C.; Otten, E. Reduction of (Formazanate)boron Difluoride Provides Evidence for an *N*-Heterocyclic B(I) Carbenoid Intermediate. *Inorg. Chem.* **2015**, *54*, 8656−8664; (b)

Barbon, S. M.; Staroverov, V. N.; Gilroy, J. B. Structurally Diverse Boron–Nitrogen Heterocycles from an $N_2O_2^{3-}$ Formazanate Ligand. *Angew. Chem. Int. Ed.* **2017**, *56*, 8173−8177.

(25) Koenig, J. D. B.; Farahat, M. E.; Dhindsa, J. S.; Gilroy, J. B.; Welch, G. C. Near-IR Absorption and Photocurrent Generation Using a First-of-its-Kind Boron Difluoride Formazanate Non-Fullerene Acceptor. *Mater. Chem. Front.* **2020**, *4*, 1643–1647.

(26) Katritzky, A. A.; Belyakov, S. A.; Cheng, D.; Durst, H. D. Syntheses of Formazans Under Phase-Transfer Conditions. *Synthesis* **1995**, *5*, 577−581.

(27) Barbon, S. M.; Staroverov, V. N.; Gilroy, J. B. Effect of Extended π Conjugation on the Spectroscopic and Electrochemical Properties of Boron Difluoride Formazanate Complexes. *J. Org. Chem.* **2015**, *80*, 5226−5235.

(28) (a) Miao, K.; Liang, M.; Wang, Z.; Zhang, C.; Sun, Z.; Xue, S. Organic Sensitizers Featuring Thiophene Derivative Based Donors with Improved Stability and Photovoltaic Performance. *Phys. Chem. Chem. Phys.* **2017**, *19*, 1927−1936; (b) Song, E.; Ha, Y. H.; Kang, B.; Yun, H.-J.; Kwon, S.-K.; Kim, Y.-H.; Cho, K. Effects of Varying the Lengths of the Donor Units in π-Extended Thienothiophene Isoindigo-Based Polymer Semiconductors. *J. Mater. Chem. C* **2018**, *6*, 9972−9980; (c) Zhang, S.; Ocheje, M. U.; Huang, L.; Galuska, L.; Cao, Z.; Luo, S.; Cheng, Y.-H.; Ehlenberg, D.; Goodman, R. B.; Zhou, D.; Liu, Y.; Chiu, Y.-C.; Azoulay, J. D.; Rondeau-Gagné, S.; Gu, X. The Critical Role of Electron-Donating Thiophene Groups on the Mechanical and Thermal Properties of Donor–Acceptor Semiconducting Polymers. *Adv. Electron. Mater.* **2019**, *5*, 1800899.

(29) (a) Kaya, E.; Balan, A.; Baran, D.; Cirpan, A.; Toppare, L. Electrochromic and Optical Studies of Solution Processable Benzotriazole and Fluorene Containing Copolymers. *Org. Electron.* **2011**, *12*, 202−209; (b) Chen, C.-P.; Wu, P.-J.; Liou, S.-Y.; Chan, Y.-H. Ultrabright Benzoselenadiazole-

Based Semiconducting Polymer Dots for Specific Cellular Imaging. *RSC Adv.* **2013**, *3*, 17507−17514; (c) Suman; Bagui, A.; Garg, A.; Tyagi, B.; Gupta, V.; Singh, S. P. A Fluorene-Core-Based Electron Acceptor for Fullerene-Free BHJ Organic Solar Cells—Towards Power Conversion Efficiencies Over 10%. *Chem. Commun.* **2018**, *54*, 4001−4004.

(30) (a) Kim, Y.; Song, C. E.; Moon, S.-J.; Lim, E. Rhodanine Dye-Based Small Molecule Acceptors for Organic Photovoltaic Cells. *Chem. Commun.* **2014**, *50*, 8235−8238; (b) He, B.; Neo, W. T.; Chen, T. L.; Klivansky, L. M.; Wang, H.; Tan, T.; Teat, S. J.; Xu, J.; Liu, Y. Low Bandgap Conjugated Polymers Based on a Nature-Inspired Bay-Annulated Indigo (BAI) Acceptor as Stable Electrochromic Materials. *ACS Sustainable Chem. Eng.* **2016**, *4*, 2797−2805; (c) Slodek, A.; Zych, D.; Maroń, A.; Golba, S.; Schab-Balcerzak, E.; Janeczek, H.; Siwy, M.; Maćkowski, S. Fluorene vs Carbazole Substituent at Quinoline Core Toward Organic Electronics. *Dyes Pigm.* **2019**, *166*, 98−106.

(31) (a) Liang, Y.; Wu, Y.; Feng, D.; Tsai, S.-T.; Son, H.-J.; Li, G.; Yu, L. Development of New Semiconducting Polymers for High Performance Solar Cells. *J. Am. Chem. Soc.* **2009**, *131*, 56−57; (b) Liang, Y.; Xu, Z.; Xia, J.; Tsai, S.-T.; Wu, Y.; Li, G.; Ray, C.; Yu, L. For the Bright Future—Bulk Heterojunction Polymer Solar Cells with Power Conversion Efficiency of 7.4%. *Adv. Mater.* **2010**, *22*, E135−E138; (c) Li, M.; Ni, W.; Wan, X.; Zhang, Q.; Kan, B.; Chen, Y. Benzo[1,2-*b*:4,5-*b*′]dithiophene (BDT)-Based Small Molecules for Solution Processed Organic Solar Cells. *J. Mater. Chem. A* **2015**, *3*, 4765−4776; (d) Tang, H.; Yan, C.; Huang, J.; Kan, Z.; Xiao, Z.; Sun, K.; Li, G.; Lu, S. Benzodithiophene-Based Small-Molecule Donors for Next-Generation All-Small-Molecule Organic Photovoltaics. *Matter* **2020**, *3*, 1403−1432.

(32) (a) Vydrov, O. A.; Scuseria, G. E. Assessment of a Long-Range Corrected Hybrid Functional. *J. Chem. Phys.* **2006**, *125*, 234109; (b) Henderson, T. M.; Izmaylov, A. F.; Scalmani, G.; Scuseria,

G. E. Can Short-Range Hybrids Describe Long-Range-Dependent Properties? *J. Chem. Phys.* **2009**, *131*, 044108.

(33) Park, W.-T.; Kim, G.; Yang, C.; Liu, C.; Noh, Y.-Y. Effect of Donor Molecular Structure and Gate Dielectric on Charge-Transporting Characteristics for Isoindigo-Based Donor–Acceptor Conjugated Polymers. *Adv. Funct. Mater.* **2016**, *26*, 4695−4703.

(34) (a) Adamo, C.; Barone, V. Toward Reliable Density Functional Methods Without Adjustable Parameters: The PBE0 Model. *J. Chem. Phys.* **1999**, *110*, 6158−6170; (b) Ernzerhof, M.; Scuseria, G. E. Assessment of the Perdew–Burke–Ernzerhof Exchange-Correlation Functional. *J. Chem. Phys.* **1999**, *110*, 5029−5036.

(35) Zhang, Z. G.; Wang, J. Structures and Properties of Conjugated Donor–Acceptor Copolymers for Solar Cell Applications. *J. Mater. Chem.* **2012**, *22*, 4178−4187.

(36) (a) Wang, J.; Shi, K.; Suo, Y.; Lin, Y.; Yu, G.; Zhan, X. Monodisperse Macromolecules Based on Benzodithiophene and Diketopyrrolopyrrole with Strong NIR Absorption and High Mobility. *J. Mater. Chem. C* **2016**, *4*, 3781−3791; (b) Bagde, S. S.; Park, H.; Lee, S.-M.; Lee, S.-H. Influence of the Terminal Donor on the Performance of 4,8-Dialkoxybenzo[1,2-*b*:4,5′]dithiophene Based Small Molecules for Efficient Solution-Processed Organic Solar Cells. *New J. Chem.* **2016**, *40*, 2063–2070; (c) Yang, L.; Zhang, S.; He, C.; Zhang, J.; Yao, H.; Yang, Y.; Zhang, Y.; Zhao, W.; Hou, J. New Wide Band Gap Donor for Efficient Fullerene-Free All-Small-Molecule Organic Solar Cells. *J. Am. Chem. Soc.* **2017**, *139*, 1958−1966.

(37) (a) Xiao, L.; Wang, H.; Gao, K.; Li, L.; Liu, C.; Peng, X.; Wong, W.-Y.; Wong, W.-K.; Zhu, X. A-D-A Type Small Molecules Based on Boron Dipyrromethene for Solution-Processed Organic Solar Cells. *Chem. Asian J.* **2015**, *10*, 1513−1518; (b) Liao, J.; Xu, Y.; Zhao, H.; Zong, Q.; Fang, Y. Novel A-D-A Type Small Molecules with *β*-Alkynylated BODIPY Flanks for Bulk

Heterojunction Solar Cells. *Org. Electron.* **2017**, *49*, 321−333; (c) Liu, W.-X.; Yao, J.-N.; Zhan, C.-L. Tailoring the Photophysical and Photovoltaic Properties of Boron-Difluorodipyrromethene Dimers. *Chin. Chem. Lett.* **2017**, *28*, 875−880.

(38) (a) Li, H.; Jäkle, F. Universal Scaffold for Fluorescent Conjugated Organoborane Polymers. *Angew. Chem. Int. Ed.* **2009**, *48*, 2313−2316; (b) Jahnke, A. A.; Howe, G. W.; Seferos, D. S. Polytellurophenes with Properties Controlled by Tellurium-Coordination. *Angew. Chem. Int. Ed.* **2010**, *49*, 10140−10144.

(39) Wen, P.; Gao, Z.; Zhang, R.; Li, A.; Zhang, F.; Li, J.; Xie, J.; Wu, Y.; Wu, M.; Guo, K. A–π–D–π–A Carbazole Derivatives with Remarkable Solvatochromism and Mechanoresponsive Luminescence Turn-On. *J. Mater. Chem. C* **2017**, *5*, 6136−6143.

(40) Gaussian 16, Revision C.01, Frisch, M. J.; Trucks, G. W.; Schlegel, H. B.; Scuseria, G. E.; Robb, M. A.; Cheeseman, J. R.; Scalmani, G.; Barone, V.; Petersson, G. A.; Nakatsuji, H.; Li, X.; Caricato, M.; Marenich, A. V.; Bloino, J.; Janesko, B. G.; Gomperts, R.; Mennucci, B.; Hratchian, H. P.; Ortiz, J. V.; Izmaylov, A. F.; Sonnenberg, J. L.; Williams-Young, D.; Ding, F.; Lipparini, F.; Egidi, F.; Goings, J.; Peng, B.; Petrone, A.; Henderson, T.; Ranasinghe, D.; Zakrzewski, V. G.; Gao, J.; Rega, N.; Zheng, G.; Liang, W.; Hada, M.; Ehara, M.; Toyota, K.; Fukuda, R.; Hasegawa, J.; Ishida, M.; Nakajima, T.; Honda, Y.; Kitao, O.; Nakai, H.; Vreven, T.; Throssell, K.; Montgomery, J. A., Jr.; Peralta, J. E.; Ogliaro, F.; Bearpark, M. J.; Heyd, J. J.; Brothers, E. N.; Kudin, K. N.; Staroverov, V. N.; Keith, T. A.; Kobayashi, R.; Normand, J.; Raghavachari, K.; Rendell, A. P.; Burant, J. C.; Iyengar, S. S.; Tomasi, J.; Cossi, M.; Millam, J. M.; Klene, M.; Adamo, C.; Cammi, R.; Ochterski, J. W.; Martin, R. L.; Morokuma, K.; Farkas, O.; Foresman, J. B.; Fox, D. J. Gaussian, Inc., Wallingford CT, 2016.

(41) Li, W.; Otsuka, M.; Kato, T.; Wang, Y.; Mori, T.; Michinobu, T. 3,6-Carbazole vs 2,7-Carbazole: A Comparative Study of Hole-Transporting Polymeric Materials for Inorganic–Organic Hybrid Perovskite Solar Cells. *Beilstein J. Org. Chem.* **2016**, *12*, 1401−1409.